



Effects of Ti doping on the electrochemical performance of $(\text{La}_{0.75}\text{Sr}_{0.25})(\text{Mn}_{0.5}\text{Cr}_{0.5})\text{O}_{3-\delta}$ anode for solid oxide fuel cells

Afizul H. Karim¹, Abdalla M. Abdalla^{2,*}, Jun-Y. Park³, Pg Mohd I. Petra¹, Abul K. Azad¹

¹Faculty of Integrated Technology, University Brunei Darussalam, Gadong B.E 1410, Negara Brunei Darussalam

²Mechanical Engineering Department, Faculty of Engineering, Suez Canal University, 41522 Ismailia, Egypt

³HMC, Green Energy Research Institute, Faculty of Nanotechnology and Advanced Materials Engineering, Sejong University, 98 Gunja-dong, Gwangjin-gu, Seoul 143-747, Republic of Korea

Received 13 March 2019; Received in revised form 16 June 2019; Received in revised form 5 September 2019;

Accepted 3 October 2019

Abstract

Single phase $\text{La}_{0.75}\text{Sr}_{0.25}\text{Mn}_{0.5}\text{Cr}_{0.5-x}\text{Ti}_x\text{O}_{3-\delta}$ (LSCMT, $0 \leq x \leq 0.3$) perovskites were investigated as possible anode material for solid oxide fuel cells with yttria stabilized zirconia (YSZ) electrolyte. LSCMT samples were synthesized by solid state reaction method and sintered at 1500 °C in air. Rietveld refinement of X-ray powder diffraction data show that the LSCMT materials crystallize in the rhombohedral symmetry with $R\bar{3}C$ space group. The cell parameters of the sample with 10 at.% of Ti ($x = 0.1$) were: $a = b = 5.5125(4) \text{ \AA}$; $c = 13.3397(6) \text{ \AA}$; $\alpha = 90^\circ$; $\beta = 90^\circ$; $\gamma = 120^\circ$. The scanning electron microscopy analyses confirmed the presence of sufficient porosity (about 35%). Symmetrical LSCMT|YSZ|LSCMT cell configurations with different Ti-doping ($x = 0.1, 0.2$ and 0.3) and good interface without delamination between the two materials, even after reduction process, were also prepared. Ti doping was very effective in reducing the interfacial polarization resistance with the lowest value of $0.22 \Omega \cdot \text{cm}^2$ and conductivity of 0.23 S/cm in 5% H_2/Ar at 800 °C. The obtained results suggest that Ti doping can substantially improve electrochemical performance of $(\text{La}_{0.75}\text{Sr}_{0.25})(\text{Mn}_{0.5}\text{Cr}_{0.5})\text{O}_{3-\delta}$ ceramics.

Keywords: perovskite, structural analysis, microstructure, impedance, solid oxide fuel cell

I. Introduction

Solid oxide fuel cell (SOFC) has drawn considerable attention of worldwide researchers in the past few decades as one of the cleanest and most efficient power generation devices [1–7]. The cell contains porous anode and cathode and a dense ionic conducting electrolyte. Electrodes should be chemically and thermally compatible with electrolyte. They should be both electronic and ionic conductors and should provide unobstructed transport of gas by means of continuous interconnected porosity. Electrodes should also possess mixed ionic and electronic conductivity with the desired catalytic activity. The electrode reactions take place at the triple phase boundaries (TPB), the interface between

the three phases, i.e. the ionic conductive, electronic conductive and gaseous phases. The larger amount of the TPB present the better the electrode performance [8,9].

A significant advantage of SOFCs lies in the high flexibility of fuel choices which allows direct utilization of hydrocarbon fuels without any pretreatment. Conventional nickel/electrolyte composite anodes show good performance using pure H_2 fuel. However, such anodes have disadvantages such as poor redox stability, carbon deposition and sulphur poisoning when used on natural gas. The nickel particles also tend to agglomerate after prolonged exposure to the fuel. These factors remain as the motivation of this research [6,10–14].

Mixed ionic and electronic conductors (MIECs) as anode materials for SOFC have attracted much attention in recent years due to their excellent resistance to sulphur poisoning and carbon deposition, high ther-

*Corresponding author: tel: +20 1032029577,
e-mail: abdalla.m.a1984@gmail.com,
abdalla.m.adalla@eng.sue.edu.eg

mochemical stability and extended triple phase boundary [15–18]. The most investigated MIEC anode materials include fluorite-type ($\text{Gd}_{0.2}\text{Ce}_{0.8}\text{O}_{2-\delta}$), perovskite-type ($\text{La}_{0.75}\text{Sr}_{0.25}\text{Cr}_{0.5}\text{Mn}_{0.5}\text{O}_{3-\delta}$), tungsten bronze-type ($\text{Sr}_{0.6}\text{Mg}_x\text{Nb}_{1-x}\text{O}_{3-\delta}$) and pyrochlore-type ($\text{Gd}_2\text{Ti}_2\text{O}_7$) materials [19–26]. In this study, we will focus on perovskite-type LSCM material due to the presence of rigid CrO_6 octahedra in the crystal structure. It enables LSCM stabilization down to low oxygen chemical potentials necessary for the SOFC anode operation, while moderate acceptor-type doping is necessary to improve electronic and ionic conduction. Nevertheless, the electrochemical performances of LSCM anodes without any additional components are essentially limited by the electronic transport leading to rather high overpotentials. The incorporation of metals (e.g. Ni or Cu) and/or electrocatalytically active additives (e.g. $\text{CeO}_{2-\delta}$) decrease electrode resistance [27]. To achieve a single phase in reducing atmosphere, it is necessary to consider the elementary chemical and physical characteristics of the elements used from the periodic table. For example, oxygen ion conduction, oxygen permeability, electronic transport characteristics, catalytic activity as well as structural properties can be adopted with increasing atomic number of the transition metal. Unfortunately, at higher temperatures, these higher atomic number transition metals suffer from phase decomposition which is unfavourable. Therefore, the substitution of Cr for Ti at the B site could improve structural stability whereas substituting Mn or Fe could enhance its catalytic effect. Based on these strategies, various single phase oxides with the form of complex perovskites $\text{ABO}_{3-\delta}$ doped with Ti and Cr were synthesized and tested. $\text{La}_{0.75}\text{Sr}_{0.25}\text{Cr}_{0.5}\text{Mn}_{0.5}\text{O}_{3-\delta}$ (LSCM), one of the potential anode materials for SOFC application under CH_4 fuel, was introduced by Tao and Irvine *et al.* [28]. LSCM showed stable performance under fuel and air conditions, where the anode polarization values measured by a three electrode set up were $0.26 \Omega \cdot \text{cm}^2$ (wet H_2), $0.51 \Omega \cdot \text{cm}^2$ (5% wet H_2) and $0.87 \Omega \cdot \text{cm}^2$ (wet CH_4) at 900°C . Excellent anode performance was also obtained from ($\text{La}_{0.75}\text{Sr}_{0.25}$) $\text{Cr}_{0.5}\text{Mn}_{0.5}\text{O}_{3-\delta}$ on $\text{La}_{0.9}\text{Sr}_{0.1}\text{Ga}_{0.8}\text{Mg}_{0.15}\text{Co}_{0.05}\text{O}_{3-\delta}$ (LSGMCo) electrolyte where the anode polarization showed a value of $0.18 \Omega \cdot \text{cm}^2$ under wet H_2 conditions at 900°C [29,30]. In this work, Cr has been substituted by Ti at the B-site to observe the physical and electrochemical properties. This is because Ti ions are stable cations and have good stability in the perovskite structure against reduction [31].

In this study, novel series of materials with the following compositions $\text{La}_{0.75}\text{Sr}_{0.25}\text{Mn}_{0.5}\text{Cr}_{0.5-x}\text{Ti}_x\text{O}_{3-\delta}$ ($x = 0.1, 0.2$ and 0.3), prepared by solid state reaction method and sintered at 1500°C , were studied using X-ray diffraction, scanning electron microscope, electrochemical impedance spectroscopy and symmetrical fuel cell test which shows promising results for future applications.

II. Materials and methods

$\text{La}_{0.75}\text{Sr}_{0.25}\text{Mn}_{0.5}\text{Cr}_{0.5-x}\text{Ti}_x\text{O}_{3-\delta}$ ($x = 0.1, 0.2$ and 0.3) powders were synthesized by solid state reaction. Stoichiometric amounts of La_2O_3 (Merck Aldrich, 99.9%), SrO (Merck Aldrich, 99.9%), MnO_2 (Sigma Aldrich, 99.9%), TiO_2 (Merck Aldrich, 99.9%) and Cr_2O_3 (Merck Aldrich, 99.9%) were mixed with ethyl alcohol and ball milled with zirconia balls for 24 h. The slurries were then put into an oven overnight at 100°C to evaporate the solvent. The obtained powders were crushed in an agate mortar and pestle. About 2.0 g of the powder was pressed into 20 mm pellet by a Kennedy hydraulic press at 10 MPa. The dark green pellets were sintered at 1200°C for 12 h by using a Nabertherm furnace. The pellets were again crushed into powders and pelleted using the same condition and sintered at final sintering temperature 1500°C for 12 h. The samples $\text{La}_{0.75}\text{Sr}_{0.25}\text{Mn}_{0.5}\text{Cr}_{0.4}\text{Ti}_{0.1}\text{O}_3$ ($x = 0.1$), $\text{La}_{0.75}\text{Sr}_{0.25}\text{Mn}_{0.5}\text{Cr}_{0.2}\text{Ti}_{0.2}\text{O}_3$ ($x = 0.2$) and $\text{La}_{0.75}\text{Sr}_{0.25}\text{Mn}_{0.5}\text{Cr}_{0.2}\text{Ti}_{0.3}\text{O}_3$ ($x = 0.3$) are identified as LSCMT1, LSCMT2 and LSCMT3, respectively.

The phase purity and crystal lattice parameters were examined at room temperature by using a Shimadzu 7000 X-ray diffractometer (XRD) using $\text{CuK}\alpha_1$ wavelength $\lambda = 0.15406 \text{ nm}$ at 40 kV and 30 mA, and a scan speed of $1.0^\circ/\text{min}$. The experimental data were refined by a Rietveld method using the Fullprof program [32]. Winplotr which is available within the Fullprof suit was used for powder diffraction data viewing and processing, peak profiling and indexing. The morphology of the prepared samples was analysed by a scanning electron microscope (SEM). SEM images were collected using a FEG-SEM (JEOL JSM-7610F) electron microscope at voltage of 2.00 kV.

Area specific resistance (ASR) values were obtained under symmetrical setup in a two electrode configuration. Anode inks were fabricated by mixing the as-prepared LSCMT in a 1:1 weight ratio with α -terpinol, Di-*n* butyl phthalate (DBP, 99% purity, Deajung Chemicals & Metals) and polyvinyl butyral (PVB, B-98, Butvar) mixture using a mortar and pestle. The anode ink was screen-printed onto both sides of the YSZ electrolyte. Active area of the anode, the working electrode, was $\sim 0.5 \text{ cm}^2$. Counter electrode (the same material as the anode) was deposited on the other side of the electrolyte. The electrodes were sintered at 1200°C for 4 h to ensure an adequate adherence with the electrolyte. The dense pellet of YSZ was bought from trusted fuel cell materials suppliers. Contacts for the electrical measurement on the anode were made using silver mesh with gold wire fixed with a small amount of platinum paste as current collector on the counter and working electrodes. AC impedance spectroscopy was carried out using an electrochemical impedance spectroscopy (EIS) with a Potentiostat/Galvanostat instrument (SP150, Bio-Logic) controlled by EC Lab impedance software. The impedance spectra of electrochemical cells (anodic part

only, ohmic resistance subtracted) were recorded at open cell voltage (OCV) with a 20 mV bias voltage over the frequency range of 10^6 to 0.1 Hz.

III. Results and discussion

3.1. Structure

Figure 1 shows the XRD patterns of the samples LSCMT1, LSCMT2 and LSCMT3 sintered at 1200 °C. The Bragg reflections shift to the right as the content of Ti increases. This can be explained by the fact that ionic radius of Ti is smaller than Cr (i.e. in 6-fold coordinated polyhedra they are 0.605 and 0.615 Å, respectively), hence spacing between layers decreases with an

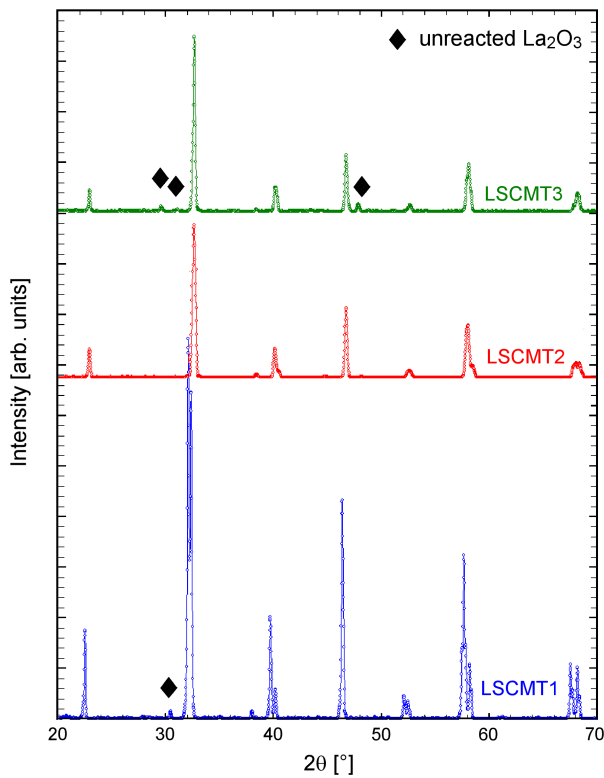


Figure 1. XRD patterns of three different compositions of LSCMT samples sintered at 1200 °C

increase in Ti content. Decrease in the value of d means an increase of θ hence the shifting of 2θ to the right. A small percentage of the second phase from unreacted La_2O_3 was observed which can be indexed as hexagonal phase ($P3m1$, JCPDS 05-0602) with unit cell parameters $a = 3.397 \text{ \AA}$ and $c = 6.129 \text{ \AA}$.

Rietveld refinement shows that all prepared $\text{La}_{0.75}\text{Sr}_{0.25}\text{Mn}_{0.5}\text{Cr}_{0.5-x}\text{Ti}_x\text{O}_{3-\delta}$ ($x = 0.1, 0.2$ and 0.3) samples crystallize in the rhombohedral symmetry with the $R\bar{3}C$ space group. The corresponding unit cell parameters and refinement factors are presented in Table 1. Figure 2 shows the Rietveld refinement of the XRD data of the sample LSCMT1 ($x = 0.1$), which corresponds to the space group $R\bar{3}C$ ($a = b = 5.5125(4) \text{ \AA}$; $c = 13.3397(6) \text{ \AA}$; $\alpha = 90^\circ$; $\beta = 90^\circ$; $\gamma = 120^\circ$). The least square refinement of the sample LSCMT1 is $\chi^2 = 1.56$ and R_f , R_p and R_{wp} values are 5.040, 21.2 and 27.4, respectively, which indicated a good fit of the experimental data. The lattice parameter also corresponds well with literature for LSCM ($a = b = 5.49914 \text{ \AA}$; $c = 13.32281 \text{ \AA}$) [33] and Ce-LSCM ($a = b = 5.5144 \text{ \AA}$; $c = 13.401 \text{ \AA}$) [34]. Since the ionic radii of Ti^{4+} and Cr^{3+} are very close, the small variation in doping percentage might have small effect on the unit cell volume. Thus, the sample where Cr was replaced with 10 at.% of Ti at the B-site gives the clear splitting of some peaks which is visible at $2\theta = 40^\circ, 53^\circ, 58^\circ$ and 68° . The observed peak splitting is related to the atomic rearrangement which makes the atomic structure in lower symmetry (rhombohedral symmetry in the $R\bar{3}C$ space group). For higher percentage of doping i.e. 20 and 30 at.%, the peak splitting decreases, but crystal phase still remains in the same symmetry and space group.

The B-site cations, which consist of Mn/Cr/Ti, are surrounded by regular octahedra of oxygen (Fig 2). These octahedra are linked together at the corner sharing three dimensional frameworks, while La/Sr ions occupy 12-coordinated A-site between these octahedra. Due to the different sizes of A and B cations, the crystal structure was distorted forcing the $(\text{Mn/Cr/Ti})\text{O}_6$ to tilt in order to optimize the La/Sr–O bond distances.

Table 1. Summary of results obtained from Rietveld analysis of X-ray diffraction data for $\text{La}_{0.75}\text{Sr}_{0.25}\text{Mn}_{0.5}\text{Cr}_{0.5-x}\text{Ti}_x\text{O}_3$ ($x = 0.1, 0.2$ and 0.3) using rhombohedral symmetry (space group $R\bar{3}C$)

Parameters	LSCMT1	LSCMT2	LSCMT3
Space group	$R\bar{3}C$	$R\bar{3}C$	$R\bar{3}C$
χ^2	1.56	0.397	0.845
a [Å]	5.5125(4)	5.5209(1)	5.5152(8)
b [Å]	5.5125(4)	5.5209(1)	5.5152(8)
c [Å]	13.3397(6)	13.4058(7)	13.4548(7)
Volume [Å ³]	351.06(1)	353.87(2)	354.42(4)
Number of fitted parameters	19	19	19
Rf factor(%)	5.04	10.9	6.76
Rp (%)	21.2	11.8	20.6
Rw (%)	27.4	17.3	28.2

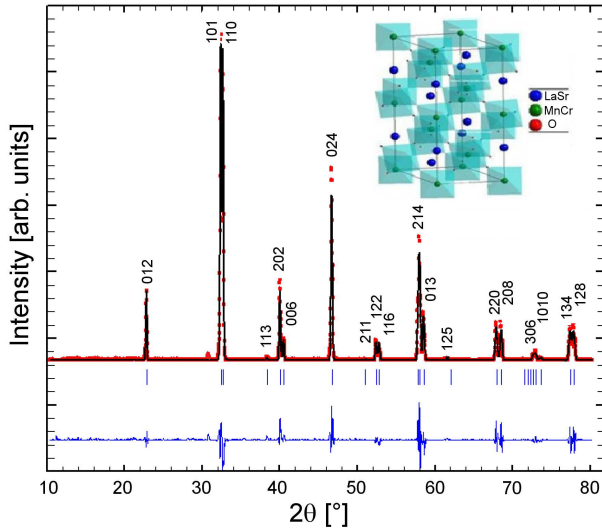


Figure 2. Observed (red dots), calculated (black line) and difference plot ($I_{obs} - I_{calc}$, blue line) of XRD intensity profiles for LSCMT ($x = 0.1$) at room temperature (short vertical lines indicate the angular position of the allowed Bragg reflections and insert is 3D schematic diagram)

The Goldschmidt tolerance factor (t) is [35]:

$$t = \frac{r_a + r_O}{\sqrt{2}(r_b + r_O)} \quad (1)$$

where r_a , r_b and r_O are the ionic radii of A-site, B-site and oxygen, respectively. For $t < 1$, the octahedra are tilted. Based on the ionic radii of La^{3+} ($r = 1.36 \text{ \AA}$), Sr^{2+} ($r = 1.44 \text{ \AA}$), Mn^{3+} ($r = 0.645 \text{ \AA}$), Cr^{3+} ($r = 0.615 \text{ \AA}$), Ti^{3+} ($r = 0.605 \text{ \AA}$) and O^{2-} ($r = 1.40 \text{ \AA}$) in appropriate coordination number, the tolerance factor was calculated to be $t = 0.91$. This indicates that the B-site octahedra of this perovskite are tilted. Octahedral tilting forces formation of crystal structure with lower symmetry.

After complete analyses of phase composition, SEM images were taken to evaluate the porosity and homogeneity of the prepared ceramics (Fig. 3). As the content of titanium increases, the grain size also increases and porosity becomes more obvious. No trace of liquid phase or secondary phase was found in the samples.

Figures 4a and 4b show the fractured cross-sectional microstructure of the symmetrical cell with dense YSZ electrolyte and porous LSCMT1 and LSCMT3 layers, respectively. The porosity increases with the increase of Ti content, which enhances gas diffusion path and increases amount of possible absorption sites. The dense YSZ electrolyte blocks gas diffusion and thus ohmic resistance decreases. The materials also show good lamination between LSCMT and YSZ and the two layers also have no delamination problem even after exposure to hydrogen gas.

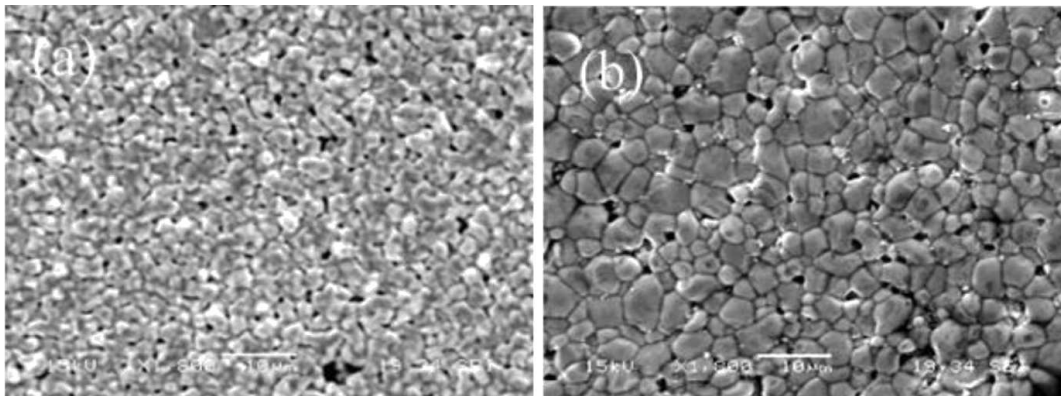


Figure 3. SEM images of samples: a) LSCMT1 and b) LSCMT3 sintered at 1200 °C

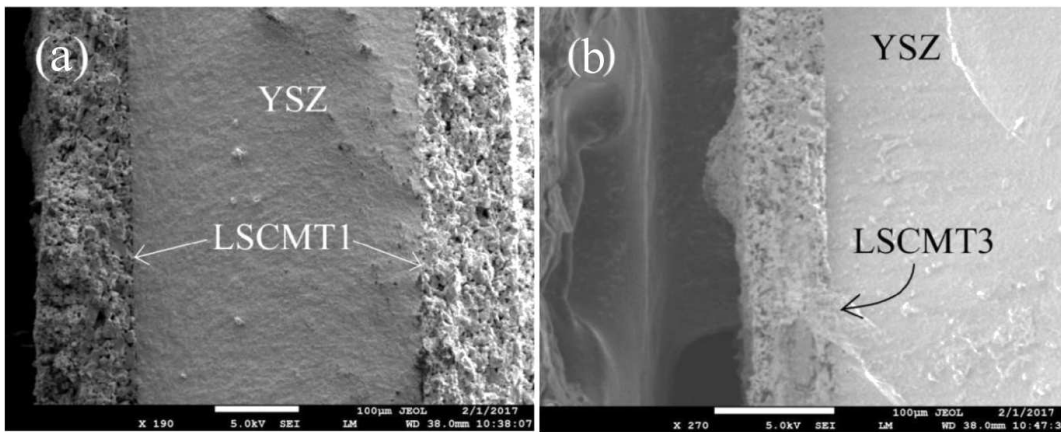


Figure 4. SEM images of the anode/electrolyte interface of samples: a) LSCMT1/YSZ and b) LSCMT3/YSZ sintered at 1200 °C for 4 h in air

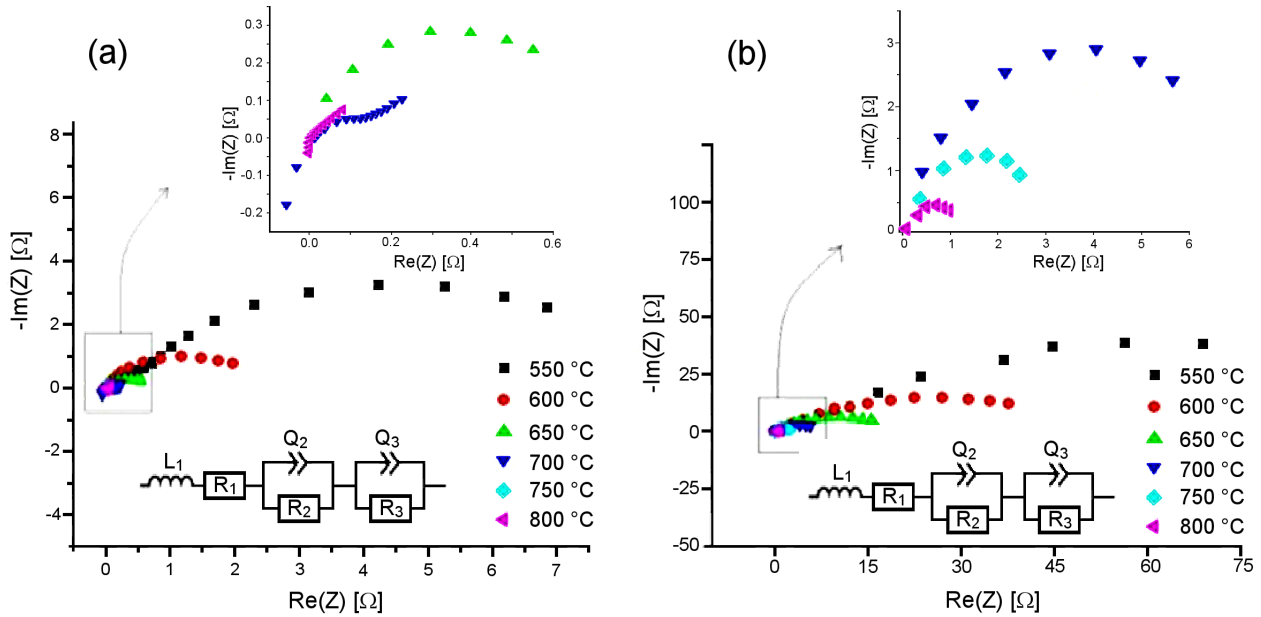


Figure 5. Anodic impedance spectra of LSCMT1 (a) and LSCMT3 (b) symmetric cells in 5% H_2/Ar at different temperatures

3.2. Electrical properties

The AC electrochemical spectroscopy (EIS) was used to determine the polarization resistance on the symmetrical LSCMT/YSZ/LSCMT cells. The equivalent circuits of the impedance spectra and the Nyquist plots are shown in Fig. 5. EC lab software was used for analysis of the experimental data. The specific area was also considered in calculating the resistivity. The arc relates to both bulk and grain boundary resistances with grain boundary being dominant at temperatures at low temperature range (below 550 °C). The bulk component only appears at reduced temperature of 550 °C. For most temperatures studied in hydrogen, there was no possibility to separate bulk and grain boundary components, so only total (bulk and grain boundary) conductivity values have been considered. The lowest impedance values were obtained in dry H_2 as fuel. Only one arc was observed hence indicates that electronic conduction was dominant. There are three parallel combinations of resistance and a constant phase element in an equivalent circuit fitting as shown in the inset of Fig. 5. Electrochemical oxidations of fuel at anode/electrolyte are affected by three different factors. Low frequency is due to the process of adsorption and diffusion of species. Intermediate frequency arc is due to the charge transfer. High frequency arc is due to the charge species transport through the surface of the anode or electrolyte. In most cases, an electrolyte supported anode symmetrical cell shows only one arc in the Nyquist plot at higher temperature. Therefore, it is important to realize that the arc consists of the sum of the all resistances and this is known as the area specific resistance (ASR). The electrochemical process involved in the fuel oxidation is the rate determining step. Impedance spectroscopy was carried out in both wet and dry hydro-

gen in the temperature range of 550–800 °C to study the conductivity behaviour. Conductivity can be examined by impedance which is a reciprocal of resistivity, i.e. small impedance pattern represent high conductivity. The small impedance reflects the smallest resistivity hence making it the composition which is the most conductive. The resistance was calculated by fitting the impedance pattern with the equivalent circuit shown as an inset in Fig. 5. Conductivity of the material can be calculated by the following equation:

$$\sigma = \frac{1}{\rho} = \frac{L}{R \cdot A} \quad (2)$$

where σ is conductivity, ρ is resistivity, L is length, R is resistance and A is cross sectional area. Equation 2 proves that resistivity is the reciprocal of conductivity and can also be expressed with the Arrhenius equation:

$$\sigma = \sigma_0 \exp\left(-\frac{E_a}{R \cdot T}\right) \quad (3)$$

where σ is conductivity, σ_0 is pre-exponential factor, E_a is activation energy, R is gas constant and T is temperature. However, it is important to note that there has been a controversy for using platinum as a current collector. Platinum paste can be regarded as catalytically active for the oxidation of hydrogen. However, the location of metal atoms is critical since the catalytic metal must be located near the triple phase boundary in order to promote the oxidation of oxygen anions coming from the electrolyte. Simple metal coating would not be optimized as LSCMs are generally low in ionic conductivity [36].

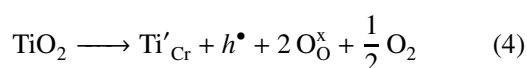
Doping with Ti has a significant effect on the impedance as shown in Fig. 5. The polarization resis-

Table 2. Conductivity [S/cm] of LSCMT1 and LSCMT3 at different temperatures in wet and dry H₂

Temperature [°C]	LSCMT1		LSCMT3	
	Wet H ₂	Dry H ₂	Wet H ₂	Dry H ₂
550	0.00	0.01	2.42×10^{-4}	3.50×10^{-4}
600	0.01	0.02	7.26×10^{-4}	1.02×10^{-3}
650	0.04	0.07	2.26×10^{-3}	2.51×10^{-3}
700	0.10	0.22	5.71×10^{-3}	6.32×10^{-3}
750	0.11	0.22	1.27×10^{-2}	1.50×10^{-2}
800	0.12	0.23	2.35×10^{-2}	3.38×10^{-2}

tance for the sample LSCMT1 at 800 °C in dry hydrogen is 0.21 Ω·cm² and conductivity is 0.23 S/cm as shown in Table 2. This value is lower than a single layer LSCM anode ($R_p = 2.3 \Omega \cdot \text{cm}^2$) and close to Ce-doped LSCM. As proposed by Lay *et al.* [34], these improvements maybe due to: i) a better adherence between the electrolyte layer and anodic layer, ii) an enhanced oxygen ionic conductivity that may increase the triple phase boundary reaction zone and/or the electrocatalytic activity of the material. The polarization resistance for the sample LSCMT3 at 800 °C in dry hydrogen is 1.42 Ω·cm² and conductivity is 0.03 S/cm which is, however, lower than for the LSCMT1 ceramics. Therefore, we can conclude that conductivity decreases with increasing Ti content.

The improved conductivity of the LSCMT1 ceramics in comparison to the LSCM can be explained from the viewpoint of defect chemistry. The point defects produced after Ti donor-doping of LSCM can be expressed with the following equation:



From this equation, it can be observed that there is a loss of lattice oxygen in a reducing atmosphere hence producing oxygen vacancies as shown by:



where Mn'_{Mn} stands for Mn^{2+} -ions on the position of Mn^{3+} ions.

IV. Conclusions

Ti-substituted LSCM has been demonstrated as an interesting improvement of the nickel-free single phase LSCM anode. $\text{La}_{0.75}\text{Sr}_{0.25}\text{Mn}_{0.5}\text{Cr}_{0.5-x}\text{Ti}_x\text{O}_{3-\delta}$ (LSCMT, $x = 0.1, 0.2$ and 0.3) were successfully synthesized by solid state reaction method and sintered at 1500 °C in air. XRD studies confirmed that the LSCMT consists of a single perovskite structure in rhombohedral symmetry (a small amount of unreacted La_2O_3 was observed in the sample sintered at 1200 °C). No structural phase change was seen while substituting Ti in the place of Cr on the B-site. SEM image shows that the porosity increases with the increase in Ti with no presence of

a liquid phase. The electrochemical impedance spectroscopy measurement indicates the lowest polarization resistance of 0.22 Ω·cm² and conductivity of 0.23 S/cm in 5% H₂/Ar for the LSCMT having $x = 0.1$. The improvements in polarization resistance and conductivity can be explained in terms of a simple defect chemistry model. Substitution of other metallic ions, such as W^{2+} , Cr^{2+} and Co^{3+} , is also another area to explore in perovskites especially for understanding the ionic and electronic transport.

Acknowledgement: The authors are grateful for University Brunei Darussalam and Suez Canal University. The author would like to thank Professor Park Jun-Young for allowing to perform this work at Sejong University, Republic of South Korea. We also acknowledge the support from the Geology Department, Faculty of Science, University Brunei Darussalam.

References

1. G. Xiao, Q. Liu, X. Dong, K. Huang, F. Chen, "Sr₂Fe_{4/3}Mo_{2/3}O₆ as anodes for solid oxide fuel cells", *J. Power Sources*, **195** (2010) 8071–8074.
2. P. Zhang, Y. H. Huang, J. G. Cheng, Z. Q. Mao, J. B. Goodenough, "Sr₂CoMoO₆ anode for solid oxide fuel cell running on H₂ and CH₄ fuels", *J. Power Sources*, **196** (2011) 1738–1743.
3. B. Ge, J.T. Ma, D. Ai, C. Deng, X. Lin, J. Xu, "Sr₂FeNbO₆ applied in solid oxide electrolysis cell as the hydrogen electrode: Kinetic studies by comparison with Ni-YSZ", *Electrochim. Acta*, **151** (2015) 437–446.
4. A. Afif, N. Radenahmad, Q. Cheok, S. Shams, J. H. Kim, A.K. Azad, "Ammonia-fed fuel cells: A comprehensive review", *Renew. Sustain. Energy Rev.*, **60** (2016) 822–835.
5. N. Radenahmad, A. Afif, P.I. Petra, S.M.H. Rahman, S.G. Eriksson, A.K. Azad, "Proton-conducting electrolytes for direct methanol and direct urea fuel cells - A state-of-the-art review", *Renew. Sustain. Energy Rev.*, **57** (2016) 1347–1358.
6. S. He, H. Dai, G. Cai, H. Chen, L. Guo, "Optimization of La_{0.75}Sr_{0.25}Cr_{0.5}Mn_{0.5}O_{3-δ}-Ce_{0.8}Sm_{0.2}O_{1.9} compositionally graded anode functional layer", *Electrochim. Acta*, **152** (2015) 155–160.
7. Z. He, X. Huang, L. Xia, Y. Yu, J. Yu, "Electrical conductivity and electrochemical performance of SrMo_{0.94}Fe_{0.06}O_{3-δ}-Gd_{0.2}Ce_{0.8}O_{1.9} composite for SOFC anode", *J. Alloys Compd.*, **660** (2016) 108–114.
8. S. Boulfrad, M. Cassidy, E. Djurado, J. T. S. Irvine, G. Jabbour, "Pre-coating of LSCM perovskite with metal catalyst

- for scalable high performance anodes”, *Int. J. Hydrogen Energy*, **38** (2013) 9519–9524.
9. T. Horita, K. Yamaji, N. Sakai, Y. Xiong, “Imaging of oxygen transport at SOFC cathode/electrolyte interfaces by a novel technique”, *J. Power Sources*, **106** (2002) 224–230.
 10. L. Dos Santos-Gómez, L. León-Reina, J.M. Porrás-Vázquez, E.R. Losilla, D. Marrero-López, “Chemical stability and compatibility of double perovskite anode materials for SOFCs”, *Solid State Ionics*, **239** (2013) 1–7.
 11. M.J. Escudero, I. Gómez de Parada, A. Fuerte, L. Daza, “Study of $\text{Sr}_2\text{Mg}(\text{Mo}_{0.8}\text{Nb}_{0.2})\text{O}_{6-\delta}$ as anode material for solid oxide fuel cells using hydrocarbons as fuel”, *J. Power Sources*, **243** (2013) 654–660.
 12. M.F. Lü, E. V. Tsipis, J.C. Waerenborgh, A.A. Yaremchenko, V.A. Kolotygin, S. Bredikhin, V.V. Kharton, “Thermomechanical, transport and anodic properties of perovskite-type $(\text{La}_{0.75}\text{Sr}_{0.25})_{0.95}\text{Cr}_{1-x}\text{Fe}_x\text{O}_{3-\delta}$ ”, *J. Power Sources*, **206** (2012) 59–69.
 13. K.G.S. Pannu, T. Pannu, T. Fürstenthaupt, V. Thangadurai, “Electrical properties of ionic liquid and double perovskite-type metal oxide composites - A new method to tailor grain-boundary impedance of ceramic electrolytes”, *Solid State Ionics*, **232** (2013) 106–111.
 14. T. Jardiell, M.T. Caldes, F. Moser, J. Hamon, G. Gauthier, O. Joubert, “New SOFC electrode materials: The Ni-substituted LSCM-based compounds $(\text{La}_{0.75}\text{Sr}_{0.25})(\text{Cr}_{0.5}\text{Mn}_{0.5-x}\text{Ni}_x)\text{O}_{3-\delta}$ and $(\text{La}_{0.75}\text{Sr}_{0.25})(\text{Cr}_{0.5-x}\text{Ni}_x\text{Mn}_{0.5})\text{O}_{3-\delta}$ ”, *Solid State Ionics*, **181** (2010) 894–901.
 15. D.K. Niakolas, “Sulfur poisoning of Ni-based anodes for solid oxide fuel cells in H/C-based fuels”, *Appl. Catal. A Gen.*, **486** (2014) 123–142.
 16. A.K. Azad, A. Hakem, P.M.I. Petra, “Titanium doped LSCM anode for hydrocarbon fuelled SOFCs”, *AIP Conf. Proc.*, **1660** (2015) 1.
 17. A. Azad, J. Zaini, P.I. Petra, L. Ming, S. Eriksson, “Effect of Nd-doping on structural, thermal and electrochemical properties of $\text{LaFe}_{0.5}\text{Cr}_{0.5}\text{O}_3$ perovskites”, *Ceram. Int.*, **42** (2016) 4532–4538.
 18. A. Ghosh, A. K. Azad, J. T. S. Irvine, “Study of Ga doped LSCM as an anode for SOFC”, *ECS Trans.*, **35** (2011) 1337–1143.
 19. J. Liu, B.D. Madsen, Z. Ji, S.A. Barnett, “A fuel-flexible ceramic-based anode for solid oxide fuel cells”, *ECS Trans.*, **5** (2002) 122–124.
 20. S. Zha, P. Tsang, Z. Cheng, M. Liu, “Electrical properties and sulfur tolerance of $\text{La}_{0.75}\text{Sr}_{0.25}\text{Cr}_{1-x}\text{Mn}_x\text{O}_3$ under anodic conditions”, *J. Solid State Chem.*, **178** (2005) 1844–1850.
 21. M. Pirzada, R.W. Grimes, L. Minervini, J.F. Maguire, K.E. Sickafus, “Oxygen migration in $\text{A}_2\text{B}_2\text{O}_7$ pyrochlores”, *Solid State Ionics*, **140** (2001) 201–208.
 22. P.R. Slater, J.T.S. Irvine, “Synthesis and electrical characterisation of the tetragonal tungsten (M = Mg, Ni, Mn, Cr, Fe, In, Sn): Evaluation as potential anode materials for solid oxide fuel cells”, *Solid State Ionics*, **124** (1999) 61–72.
 23. S. Hui, A. Petric, “Evaluation of yttrium-doped SrTiO_3 as an anode for solid oxide fuel cells”, *J. Eur. Ceram. Soc.*, **22** (2002) 1673–1681.
 24. X. Li, H. Zhao, X. Zhou, N. Xu, Z. Xie, N. Chen, “Electrical conductivity and structural stability of La-doped SrTiO_3 with A-site deficiency as anode materials for solid oxide fuel cells”, *Int. J. Hydrogen Energy*, **35** (2010) 7913–7918.
 25. X. Zhu, Z. Lu, B. Wei, Y. Zhang, X. Huang, W. Su, “Co-impregnated yttria-stabilized zirconia anode for single-chamber solid oxide fuel cells”, *Int. J. Hydrogen Energy*, **35** (2010) 6897–6904.
 26. L. Zhang, S. Ping, H. Quan, X. Chen, J. Ma, X. Chao, “A comparative study of H_2S poisoning on electrode behavior of Ni/YSZ and Ni/GDC anodes of solid oxide fuel cells”, *Int. J. Hydrogen Energy*, **35** (2010) 12359–12368.
 27. X.J. Chen, Q.L. Liu, K.A. Khor, S.H. Chan, “High-performance $(\text{La,Sr})(\text{Cr,Mn})\text{O}_3/(\text{Gd,Ce})\text{O}_{2-\delta}$ composite anode for direct oxidation of methane”, *J. Power Sources*, **165** (2007) 34–40.
 28. S. Tao, J.T.S. Irvine, “A redox-stable efficient anode for solid-oxide fuel cells”, *Nature Mater.*, **2** (2003) 320–323.
 29. J. Jeong, A.K. Azad, H. Schlegel, B. Kim, S.W. Baek, K. Kim, H. Kang, J.H. Kim, “Structural, thermal and electrical conductivity characteristics of $\text{Ln}_{0.5}\text{Sr}_{0.5}\text{Ti}_{0.5}\text{Mn}_{0.5}\text{O}_{3-\delta}$ (Ln: La, Nd and Sm) complex perovskites as anode materials for solid oxide fuel cell”, *J. Solid State Chem.*, **226** (2015) 154–163.
 30. S. Jiang, X. Chen, S. Chan, J. Kwok, K. Khor, “ $(\text{La}_{0.75}\text{Sr}_{0.25})(\text{Cr}_{0.5}\text{Mn}_{0.5})\text{O}_3/\text{YSZ}$ composite anodes for methane oxidation reaction in solid oxide fuel cells”, *Solid State Ionics*, **177** (2006) 149–157.
 31. W. Li, Y. Cheng, Q. Zhou, T. Wei, Z. Li, H. Yan, Z. Wang, X. Han, “Evaluation of double perovskite $\text{Sr}_2\text{FeTiO}_{6-\delta}$ as potential cathode or anode materials for intermediate-temperature solid oxide fuel cells”, *Ceram. Int.*, **41** (2015) 12393–12400.
 32. J. Rodriguez-Carvajal, “Recent advances in magnetic structure determination neutron powder diffraction”, *Physica B*, **192** (1993) 55–69.
 33. S. Xu, S. Chen, M. Li, K. Xie, Y. Wang, Y. Wu, “Composite cathode based on Fe-loaded LSCM for steam electrolysis in an oxide-ion-conducting solid oxide electrolyser”, *J. Power Sources*, **239** (2013) 332–340.
 34. E. Lay, G. Gauthier, S. Rosini, C. Savaniu, J.T.S. Irvine, “Ce-substituted LSCM as new anode material for SOFC operating in dry methane”, *Solid State Ionics*, **179** (2008) 1562–1566.
 35. S. Hossain, A.M. Abdalla, S. Noorazeen Binti Jamain, J.H. Zaini, “A review on proton conducting electrolytes for clean energy and intermediate temperature-solid oxide fuel cells”, *Renew. Sustain. Energy Rev.*, **79** (2017) 750–764.
 36. E. Lay, L. Dessemond, G. Gauthier, “Ba-substituted LSCM anodes for solid oxide fuel cells”, *J. Power Sources*, **221** (2013) 149–156.